Soft Matter

Cite this: *Soft Matter*, 2011, **7**, 10812

www.rsc.org/softmatter

PAPER

Electrospinning of nanofibres with parallel line surface texture for improvement of nerve cell growth†‡

Chen Huang,[ab] Yanwei Tang,[b] Xin Liu,[b] Alessandra Sutti,[b] Qinfei Ke,[a] Xiumei Mo,[a] Xungai Wang,[b] Yosry Morsi[c] and Tong Lin*[b]

Received 27th July 2011, Accepted 24th August 2011
DOI: 10.1039/c1sm06430d

Nanofibres having a parallel line surface texture were electrospun from cellulose acetate butyrate solutions using a solvent mixture of acetone and *N*,*N*′-dimethylacetamide. The formation mechanism of the unusual surface feature was explored and attributed to the formation of voids on the jet surface at the early stage of electrospinning and subsequent elongation and solidification of the voids into a line surface structure. The fast evaporation of a highly volatile solvent, acetone, from the polymer solution was found to play a key role in the formation of surface voids, while the high viscosity of the residual solution after the solvent evaporation ensured the line surface to be maintained after the solidification. Based on this principle, nanofibres having a similar surface texture were also electrospun successfully from other polymers, such as cellulose acetate, polyvinylidene fluoride, poly(methyl methacrylate), polystyrene and poly(vinylidene fluoride-*co*-hexafluoropropene), either from the same or from different solvent systems. Polarized Fourier transform infrared spectroscopy was used to measure the polymer molecular orientation within nanofibres. Schwann cells were grown on both aligned and randomly oriented nanofibre mats. The parallel line surface texture assisted in the growth of Schwann cells especially at the early stage of cell culture regardless of the fibre orientation. In contrast, the molecular orientation within nanofibres showed little impact on the cell growth.

Electrospinning is an effective technique to produce polymer nanofibres.[1] It involves using a strong electrical field to rapidly stretch a polymer solution into fine filaments. The solvent evaporation from the filaments leads to the formation of dry or semi-dry fibres, which deposit randomly on the collector forming a nonwoven mat in most cases. Nanofibres produced from electrospinning have a large specific-surface-area and can be functionalised easily through an electrospinning process. They have emerged as exciting candidates for wide applications in areas as diverse as tissue engineering, filtration, energy conversion and storage, reinforcement, sensor and many others.[1,2]

In general, electrospun nanofibres have a circular cross-section with a smooth fibre surface. Depending on the spinneret structure, collecting mode and electrospinning condition, they can have aligned fibrous structures,[3] bicomponent cross-sectional configurations,[4] ribbon shapes[5] or porous surfaces.[6] Previously, we have found that a POSS (polyhedral oligomeric silsesquioxane)-containing copolymer can be electrospun into coarse fibres with a nano-fibril secondary structure,[7] which endows the fibres with a strider leg-like surface topology and high superhydrophobicity with a very low contact angle hysteresis. However, the detailed mechanism governing the formation of such an interesting structure is still unclear, which hampers the development of nanofibres having similar structure features.

It has been established that fibres with a rough surface are conducive to cell adhesion as they provide more topographical cues.[8] The feasibility of using fibrous webs, especially those containing aligned nanofibres, as scaffolds for peripheral nerve repair has been explored recently.[9] Structurally, nanofibre webs are more comparable to the native tissue scaffolds, *i.e.* extracellular matrices (ECMs),[10] and should give better support to cell growth,[11] compared to the conventional fibres of a similar structure. Moreover, fibre morphology has been found to play an important role in affecting the growth and functions of nerve cells.[12] The recovery period of peripheral nerve system could be further shortened when the scaffold has an aligned fibre

[a]*State Key Laboratory for Modification of Chemical Fibers and Polymer Materials, College of Textiles, Donghua University, Shanghai, 201620, China*
[b]*Centre for Material and Fibre Innovation, Deakin University, Geelong, Vic 3217, Australia. E-mail: tong.lin@deakin.edu.au*
[c]*Biomechanical and Tissue Engineering Group, Faculty of Engineering and Industrial Sciences, Swinburne University, Hawthorn, Vic 3122, Australia*
† Electronic supplementary information (ESI) available: Experimental details, SEM images, polarized FTIR spectra, WAXs patterns and calculation of the surface area. See DOI: 10.1039/c1sm06430d
‡ The authors thank Dr Rupinder Kanwar and Dr Cynthia Wong for their kind support to the cell culture work, and Dr Zhiguang Xu for his valuable assistance in analysing the CAB conformation. Scholarship for the first author from the China Scholarship Council is acknowledged.

arrangement. Nanofibres having a secondary oriented structure on the surface should be beneficial towards cell adhesion and oriented growth, which has not yet been demonstrated in the research literature.

In the recent study, we have found that nanofibres having a parallel line surface texture can be electrospun from cellulose acetate butyrate (CAB). By examining the solution properties and nanofibre morphologies, we have elucidated their formation mechanism, and based on this produced similar nanofibres successfully from other polymers. The parallel line surface textures provide support to the growth of nerve cells even if the fibres are not oriented. Herein, we report on electrospinning of these novel nanofibres and the growth performance of Schwann cells on the nanofibre mats.

Fig. 1 shows the typical morphologies of CAB fibres electrospun from CAB–acetone/DMAc (2 : 1, v/v) solutions (for experimental details, see ESI†). The CAB concentration influenced both the fibre morphology and the surface feature. When the CAB concentration was lower than 12 wt%, beaded fibres were produced. The fibres became uniform when the CAB concentration was higher. With an increase in the CAB concentration, fibre diameter increased. Fibres with a smooth surface were produced when the CAB concentration was low. Parallel lines appeared on the fibre surface when the CAB concentration was increased to 12 wt%. Such a secondary surface structure became more evident when CAB concentration was larger than 15 wt%.

When CAB concentration was maintained the same (*e.g.* 15 wt%) while the volume ratio of the solvents acetone and DMAc varied in the solution, the fibre morphology and surface feature changed (see ESI†). Decreasing the acetone content led to decreased fibre average diameter and blurred surface line texture. When the acetone/DMAc ratio was 9/1 (v/v), the surface lines with explicit gaps were generated on the as-spun fibres, and the line width was below 100 nm. The line width increased to about 200 nm when the acetone/DMAc ratio was 2/1 (v/v). Further decreasing the acetone content (*e.g.* acetone/DMAc ratio, 1 : 2 v/v) led to the disappearance of the surface line feature. Here it should be noted that 15 wt% CAB solution using pure acetone or DMAc as solvent cannot be electrospun into fibres.

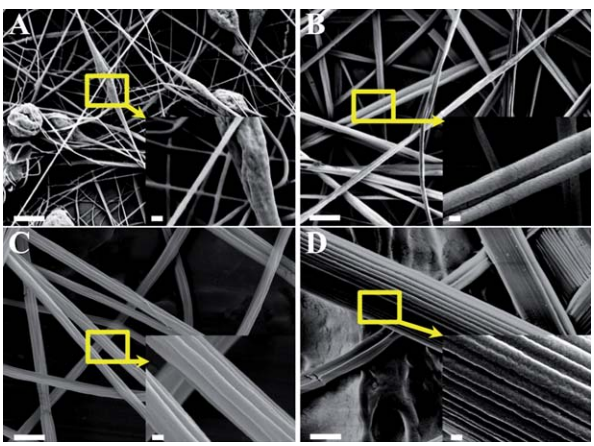

Fig. 1 CAB fibres electrospun from (A) 5 wt%, (B) 12 wt%, (C) 15 wt%, and (D) 30 wt% (grams in 100 ml solvent) CAB solutions (solvent, acetone/DMAc = 2/1, v/v). Scale bar (main picture) = 2 μm, scale bar (inset) = 200 nm.

Fig. 2 illustrates the effect of electrospinning distance on the fibre surface morphology. When the electrical field was kept at 1 kV cm^{-1}, changing the electrospinning distance led to variation in the fibre surface morphology (Fig. 2A–C). At a short spinning distance (14 cm), the resulting fibres had an inter-bonded structure. The fibre surface looked smooth and there were almost no parallel lines recognised (Fig. 2A). The parallel line surface texture became obvious when the spinning distance was between 17 cm and 20 cm (Fig. 2B and C). The formation of bonded fibres at a low electrospinning distance was attributed to the insufficient evaporation of solvent from the fibres.

For comparison, the CAB solution was fed off the nozzle at the same flow rate without applying the high voltage. Once the solution was pressed out and exposed to air, elliptical pores were induced to form, which can be observed on the dried solution under SEM (Fig. 2D). When the solution at the nozzle tip was stretched manually into a thick filament, ripples were formed on

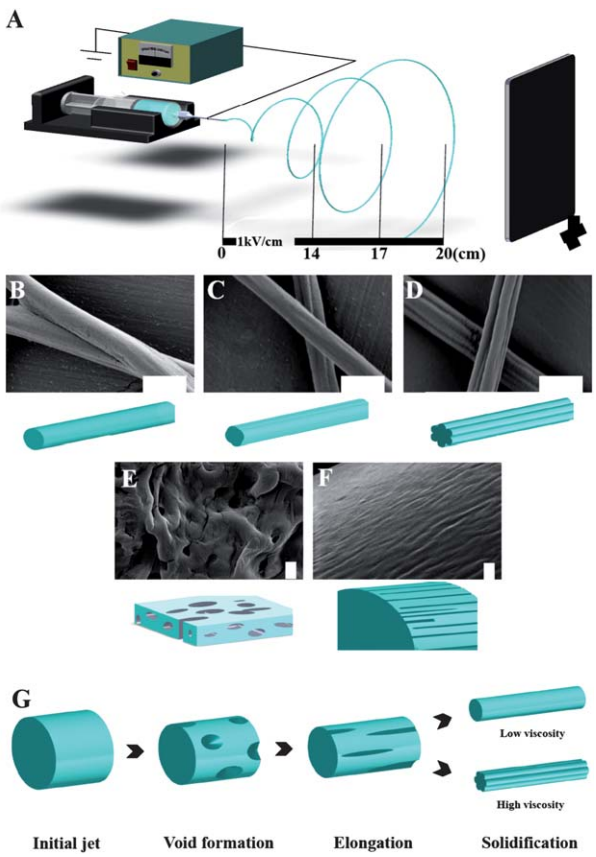

Fig. 2 A) Schematic diagram of the electrospinning process. (B–D) SEM and schematic images of CAB fibres produced from different electrospinning distances (electrical field intensity, 1 kV cm^{-1}), (B) 14 cm, (C) 17 cm, and (D) 20 cm. The schematic images are drawn based on the corresponding SEM images to illustrate the fibre morphologies. (E) SEM and schematic images of the CAB solution solidified on the nozzle tip. (F) SEM and schematic images of CAB fibre prepared by stretching the CAB solution manually from the nozzle tip. (G) Proposed formation mechanism of the parallel line fibre surface structure. Scale bars in the SEM images = 500 nm.

the filament surface (Fig. 2E). The formation of the ripple-like surface structure could come from the pores formed on the liquid surface due to the solvent evaporation from the CAB solution and subsequent elongation.

To explore the formation mechanism of the unusual parallel line surface morphology on the electrospun CAB fibres, the solvent evaporation from the CAB solution was examined. It was found that a rough surface was developed rapidly on the solution surface when the CAB solution was exposed to air. The formation of the rough surface on the polymer solution surface has been widely studied and explained as the rapid evaporation of a high volatile solvent from the polymer fluid.[13] For the CAB solution in acetone/DMAc, the evaporation of the acetone and subsequent transformation of acetone-rich region into voids could be the main reason leading to the porous surface.

The formation of the rough surface can be traced by the confocal microscope. Fig. 3A–C shows the confocal microscopic images of a small volume of 15 wt% CAB solution on a glass slide. In the natural convection condition, the liquid film was initially transparent having a smooth surface (Fig. 3A). In 30 seconds, the liquid film became opaque, and small voids accompanied with several large pores (diameter around 10 μm) were formed on the solution surface (Fig. 3B). Leaving the liquid film further in the ambient environment for 30 seconds led to a highly porous surface (Fig. 3C).

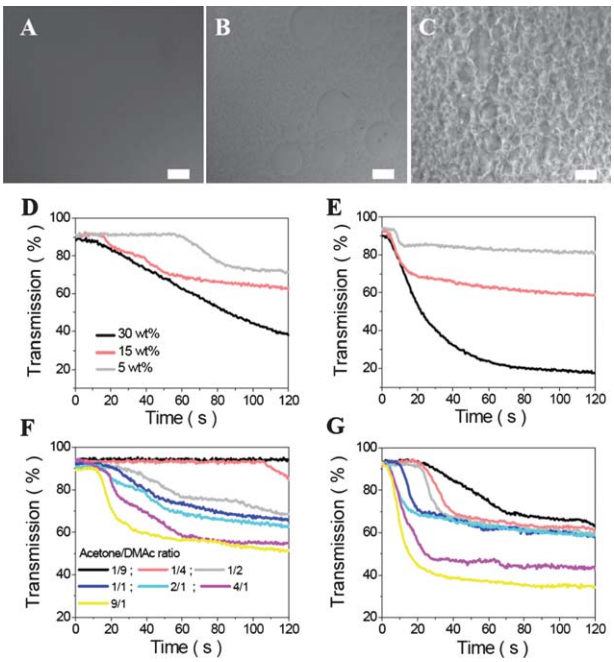

Fig. 3 (A–C) Confocal microscopic images of 15 wt% CAB solution: (A) just dropping on the glass slide, (B) after 30 seconds under the natural convection condition, and (C) after 60 seconds under the natural convection condition. (D and E) Transmittance–time curves of CAB solutions under (D) natural convection condition at room temperature and (E) in air flow (speed, 1.5 m s^{-1}, room temperature), (F and G) transmittance–time curves of 15 wt% CAB solution with different acetone/DMAc ratios under (F) natural convection condition at room temperature and (G) in air flow (speed, 1.5 m s^{-1}, room temperature). Scale bar in A–C, 10 μm.

Since the formation of the rough surface is accompanied with the transparency decrease, the optical transmittance of the thin solution film (initial thickness = 90 μm) was recorded. Fig. 3D shows the typical transmittance–time curves of CAB solutions (solvent: acetone/DMAc, 2 : 1 v/v) under a natural convection condition at room temperature. For 5 wt% CAB solution, the transmittance changes evidently experienced three stages: slow reduction, fast decrease and final stabilisation. The first stage was associated with a rapid evaporation of solvent from the surface zone and formation of wet pores. At the second stage, the solvent evaporation was accelerated because the porous surface increased the solvent evaporation area. The final stabilisation was related to the formation of stable pores and a porous structure. The first stage for 5 wt% CAB took about 60 seconds. In comparison, 15 wt% CAB had a much shorter first stage, around 20 seconds. For 30 wt% CAB solution, the three stages became indistinct under the natural convection condition. This is presumably because the thicker solution contains less volume of solvent to evaporate, and higher polymer concentration generates a larger viscoelastic force to slow down the void formation.

The void formation was accelerated when the solvent evaporation was performed under an enhanced convection condition. Fig. 3E shows the transmittance–time curves of the CAB solution films in an air flow (speed, 1.5 m s^{-1}) environment at room temperature. The transmittance changes showed the clearly identified evaporation stages for all the solution films (initial thickness = 90 μm). In comparison with 15 wt% and 30 wt% CAB solutions, 5 wt% CAB stayed longer in the first stage, but shorter in the second stage. It was interesting to note that the time period required for the 15 wt% CAB solution to reach the final-stabilisation stage was similar to that for 5 wt% CAB solution. Since the jet performs a high-speed whipping movement (100–300 m s^{-1}) during electrospinning,[14] the solvent evaporation from the jet/filament during electrospinning is much faster in this enhanced convection condition, thus taking a much shorter time to form voids.

The void formation was also affected by acetone/DMAc ratio. For 15 wt% CAB solution, the influence of acetone/DMAc ratio on the transmittance–time curve is shown in Fig. 3F and G. Under both natural and enhanced convection conditions, higher acetone content tended to take a shorter period for the solution to reach the final stabilisation stage.

Based on the electrospinning results and the solvent evaporation performance of the CAB solution, we proposed the formation mechanism of a parallel line surface structure on the electrospun fibres. As schematically illustrated in Fig. 2G, voids are initially formed on the jet surface at the early electrospinning stage due to the strong convection and instantaneous evaporation of acetone from the filament; with elongation of the filaments, the voids are highly stretched to form oriented lines on the filament surface. The complete evaporation of the solvent at the final stage of electrospinning results in solid fibres with the line surface texture fixed.

Under the same electrical field intensity, the jet is expected to be stretched at the similar strain rate and velocity.[15] A short electrospinning distance (*e.g.* 14 cm) suggests insufficient stretching and solvent evaporation. As a result of solvent residue in the filaments and associated increase in the flexibility, the elongated voids, *i.e.* the surface parallel lines, tended to be

smoothened due to the action of the surface tension. A longer electrospinning distance provides the jet with longer stretching and solvent evaporation time, facilitating the formation of the surface line structure, which is in accordance with our experimental finding.

It should be noted that CAB in DMAc often forms a highly viscous solution. Providing acetone evaporates completely from the 15 wt% CAB solution (acetone/DMAc, 2 : 1, v/v), if no DMAc is co-evaporated with the acetone, the resulting solution should contain 45 wt% CAB. We found that DMAc solution having such a high concentration of CAB behaved like a gel, having a high viscosity (52.4 kP). In practice, CAB should have higher concentration because of the co-evaporation of DMAc with acetone during the formation of the porous surface. The high viscosity and low flexibility of the residual solution is another reason for the formation of solid parallel lines on the nanofibre surface. This can also be used to explain the experimental result that the nanofibres electrospun from the CAB solutions of concentration below 12 wt% show no parallel line surface feature. Although a dilute CAB solution was easy to be stretched because of its low viscosity, the relatively low viscosity of the residual fluid after the evaporation of acetone enabled the filaments to have a smooth surface.

It was also found that the molecular weight of CAB influenced the formation of the parallel line surface (see ESI†). In the above experiments, the CAB having a viscosity average molecular weight (M_η) of 70 000 was used. When CAB of a lower molecular weight ($M_\eta \approx 30\,000$) was employed, in the same solvent system (acetone/DMAc, 2 : 1 v/v) even at a high CAB concentration (*e.g.* 30 wt%) for electrospinning, fibres with a smooth surface were still produced because of the low viscosity (53.35 P) in the residual solution.

To further examine the effect from solvents, DMAc and acetone were replaced with DMF and methanol for electrospinning. CAB fibres electrospun from acetone/DMF had a similar surface feature to those from acetone/DMAc (see ESI†), indicating that DMAc and DMF played a similar role in the electrospinning of CAB nanofibres. However, surface lines, although still existing, became less apparent when acetone was replaced with methanol.

In addition, a few other polymers that are soluble in acetone and DMAc, such as cellulose acetate, polyvinylidene fluoride, poly(methyl methacrylate) and polystyrene, were electrospun using an acetone and DMAc (ratio, 2/1 v/v) solvent system. It was interesting to reveal that all the as-spun fibres had a similar parallel line surface feature (see ESI†), demonstrating the universality of this method to electrospin polymer fibres with ordered secondary surface structures.

Other polymers such as polystyrene (PS), polycaprolatone (PCL), and poly(vinylidene fluoride-*co*-hexafluoropropene) (PVDF-HFP) that are soluble in the mixtures of two solvents having different boiling points were also tested. For PS (solvents: DCM/DMF) and PVDF-HFP (solvents: THF/DMF), fibres with parallel line surfaces were produced in the suitable conditions (see ESI†). However, smooth PCL nanofibres without line surface structures were always resulted although the solvents (DCM/DMF and THF/DMF) used in the polymer solutions had a large difference in the boiling points (see ESI†). This suggests that polymer type could be another important factor affecting the formation of surface parallel line, which warrants for further study.

With the aid of a high speed rotating mandrel, aligned CAB nanofibres with line surface structures were produced (see ESI†). Slightly different to those that were collected using a stationary collector, the parallel line surface texture appeared on the fibres that were electrospun at a shorter distance (*e.g.* 14 cm). This is probably because the high speed mandrel collector further enhances the convection, which accelerates the solvent evaporation from the jet/filaments.

Apart from the ordered surface feature, the molecular orientation within nanofibres was also examined. Fig. 4 shows the polarized FTIR spectra of randomly oriented and aligned CAB fibre mats at angles 0, 30, 60 and 90°. For the randomly oriented CAB nanofibre mat, the initial angle (0°) was set randomly, and the spectra showed almost no dependence on the sample angle (Fig. 4A). For the aligned CAB nanofibre mat, the initial angle was set to make the fibre alignment in the same direction as that of the polarized IR light source. The FTIR spectrum changed the profile with sample angle, and the largest difference came from the sample angles between 0 and 90° (Fig. 4B). This suggests the orientation of CAB molecules within the nanofibres.

Table 1 lists the assignment of main vibration peaks and dichroic ratio, $R = A^{\parallel}/A^{\perp}$, where $A^{\parallel}$ and $A^{\perp}$ are the polarized infrared absorption intensity of a particular vibration in the parallel ($\theta = 0°$) and perpendicular ($\theta = 90°$) directions, respectively. $R = 1$ suggests the equal distribution of the vibration in both parallel and perpendicular directions along the fibre length, while R = infinity indicates a perfect orientation along the fibre length direction.[16]

As expected, all dichroic ratios (0.88–0.98) for the randomly oriented nanofibre mat were close to 1. However, for the aligned CAB nanofibre mat, the peaks at 1367, 1163, 1070 and 920 cm^{-1}, which corresponded to C–H bending, C–O–C asymmetric stretching, C–O–C stretching and ring asymmetric stretching,

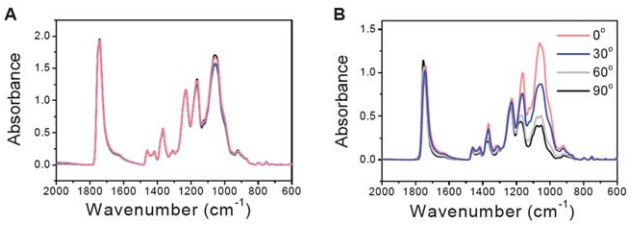

Fig. 4 Polarized FTIR spectra of (A) randomly oriented CAB nanofibres and (B) aligned CAB nanofibres (electrospinning distance, 20 cm).

Table 1 Vibrations and dichroic ratios of CAB fibres

		Dichroic ratio (R)	
υ/cm^{-1}	Vibrations (ref. 17)	Random	Oriented
1745	νC=O (carboxylate)	0.98	0.95
1367	δsC–H	0.95	1.96
1230	νC–O (carboxylate)	0.99	1.15
1163	νasC–O–C (bridge)	0.92	2.44
1070	νC–O–C (pyranose ring)	0.91	3.49
920	νas (ring)	0.88	3.43

had higher R values. This suggests that the pyranose rings in the polymer main-chain orient along the fibre length direction. Such a molecular orientation was largely dependent on the fibre stretching degree during electrospinning. Molecular orientation in nanofibres was enhanced when the applied voltage was increased or longer spinning distance was used for electrospinning (ESI†). It was also interesting to note that the peaks at 1745 and 1230 cm^{-1}, which were assigned to the C=O and C–O stretching of carboxyl groups, had an R value close to 1. This indicates that the carboxyl groups in the CAB fibres have no direction preference, which presumably comes from the rotation of the side-chains butyryl and acetyl groups of CAB molecules.

Both randomly oriented and aligned electrospun CAB nanofibre mats, either with parallel line or with smooth fibre surface, were used as scaffolds to culture rat Schwann cells. Fig. 5 shows the confocal microscope images of the cells on these nanofibre mats after different culture periods. On the aligned CAB fibre mats, the cell growth was found to experience three discernible stages: initial adhesion, spreading and alignment/proliferation no matter if the fibres had a parallel line structure surface (Fig. 5A and C). After 8 hours of culture, the cells growing on fibres that had the surface line structure showed elongated cell cytoskeleton and nuclei (Fig. 5A), while the cells on the smooth fibres looked less stretched. At day 4, the cells aligned with the elongated cytoskeleton and nuclei along the fibre direction (Fig. 5A and C). At day 7, the whole scaffold was filled with aligned cells

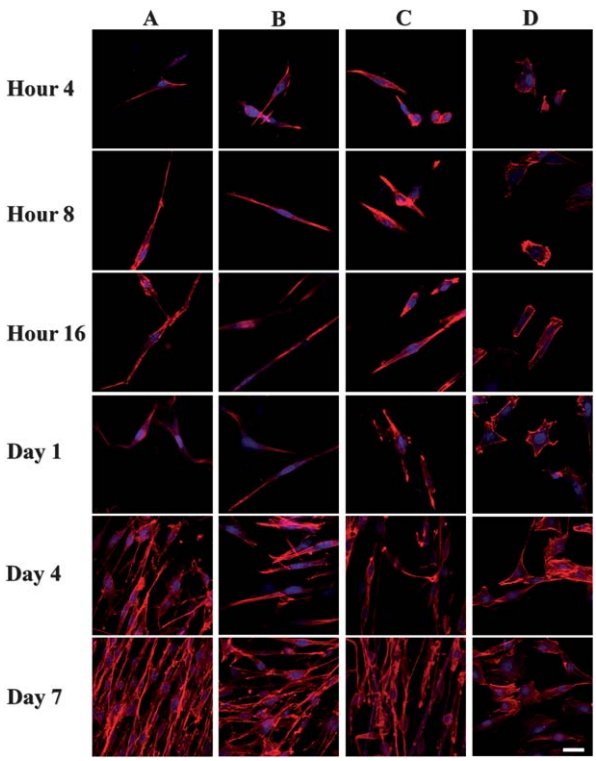

Fig. 5 Typical confocal microscopic images of Schwann cells grown on (A) aligned CAB nanofibres having a parallel line surface texture, (B) randomly oriented CAB nanofibres having a parallel line surface texture, (C) aligned CAB nanofibres having a smooth surface, and (D) randomly oriented CAB nanofibres having a smooth surface, in different culture periods. Scale bar = 25 μm.

suggesting the prompt proliferation. In comparison with the cells on the smooth nanofibres, the cells on the nanofibres having a parallel line surface structure showed a slightly better alignment. The parallel line surface structure could facilitate the cell extension at the early stage of cell culture.

More evident impact from the fibre surface line structure can be found on the randomly oriented CAB nanofibre mats (Fig. 5B and D). The cells on the nanofibres with a parallel line surface were extended into bipolar shapes. Long protoplasmic filaments had already formed on some cells after 8 hours of culture. At day 7, full grown protoplasmic filaments were clearly observed in the micrograph of the sample, which was similar to those that grew on the aligned CAB nanofibres except that the cells were less oriented (Fig. 5B). The cells on the smooth nanofibres, however, presented a multipolar morphology regardless of the culturing period (Fig. 5D).

Obviously, both the fibre alignment and the secondary parallel line structure assisted in the cell growth, especially the elongation of Schwann cells. Schwann cells showed an early adherence on the parallel lined scaffolds as the majority of the cells exhibited a typical Schwann cell morphology with elongated cell bodies and protoplasmic filaments within the first day of culture. However, when the cell grew on the fibres with a smooth surface, especially on randomly oriented smooth fibres, longer time was required for the attachment and elongation of cells.

The parallel line morphology on the fibre surface not only provided ordered topographical cues but also increased the surface area. Using a simple model, we have estimated the surface area of a nanofibre having parallel line surface structures (see ESI†). For a given weight of fibres, the parallel lines can increase the fibre surface area by 30%. The increased surface area could enhance the cell adhesion, which is another benefit of the secondary ordered fibre surface texture to cell culture.

The molecular orientation within the CAB nanofibres seemed to have little influence on the cell growth because all fibre samples, including the randomly oriented fibre mat having smooth fibre surface, contained oriented CAB molecules within the fibres (see ESI†).

In conclusion, CAB nanofibres having a novel parallel line surface texture have been electrospun successfully. The formation of this special surface morphology was attributed to the formation of voids on the jet/filament surface at the early electrospinning stage and subsequent elongation and solidification of the voids to form surface lines in the later electrospinning process. The fast evaporation of a highly volatile solvent, acetone, from the polymer solution plays a key role in the formation of surface voids, while the high viscosity of the residual solution after acetone evaporation ensures the surface lines to be maintained. The parallel line surface topographic cues provided by the nanofibres assist in the growth of Schwann cells, which may open new ways to culture nerve cells for neural tissue engineering and repairs.

Notes and references

1 D. Li and Y. Xia, *Adv. Mater.*, 2004, **16**, 1151–1170.
2 H. Cao, T. Liu and S. Y. Chew, *Adv. Drug Delivery Rev.*, 2009, **61**, 1055–1064; S. Ramakrishna, K. Fujihara, W.-E. Teo, T. Yong, Z. Ma and R. Ramaseshan, *Mater. Today*, 2006, **9**, 40–50; X. Wang, C. Drew, S. H. Lee, K. J. Senecal, J. Kumar and

L. A. Samuelson, *Nano Lett.*, 2002, **2**, 1273–1275; M. M. Bergshoef and G. J. Vancso, *Adv. Mater.*, 1999, **11**, 1362–1365.
3 D. Li, Y. Wang and Y. Xia, *Nano Lett.*, 2003, **3**, 1167–1171.
4 Y. Zhang, Z.-M. Huang, X. Xu, C. T. Lim and S. Ramakrishna, *Chem. Mater.*, 2004, **16**, 3406–3409; T. Lin, H. Wang and X. Wang, *Adv. Mater.*, 2005, **17**, 2699–2703.
5 S. Koombhongse, W. Liu and D. H. Reneker, *J. Polym. Sci., Part B: Polym. Phys.*, 2001, **39**, 2598–2606.
6 M. Bognitzki, W. Czado, T. Frese, A. Schaper, M. Hellwig, M. Steinhart, A. Greiner and J. H. Wendorff, *Adv. Mater.*, 2001, **13**, 70–72.
7 Y. Xue, H. Wang, D. Yu, L. Feng, L. Dai, X. Wang and T. Lin, *Chem. Commun.*, 2009, 6418–6420.
8 M. M. Stevens and J. H. George, *Science*, 2005, **310**, 1135–1138.
9 S. Y. Chew, R. Mi, A. Hoke and K. W. Leong, *Adv. Funct. Mater.*, 2007, **17**, 1288–1296; Y. I. Cho, J. S. Choi, S. Y. Jeong and H. S. Yoo, *Acta Biomater.*, 2010, **6**, 4725–4733; S. H. Lim, X. Y. Liu, H. Song, K. J. Yarema and H. Q. Mao, *Biomaterials*, 2010, **31**, 9031–9039; X. Liu, J. Chen, K. J. Gilmore, M. J. Higgins, Y. Liu and G. G. Wallace, *J. Biomed. Mater. Res., Part A*, 2010, **94**, 1004–1011; M. P. Prabhakaran, J. R. Venugopal, T. T. Chyan, L. B. Hai, C. K. Chan, A. Y. Lim and S. Ramakrishna, *Tissue Eng. A*, 2008, **14**, 1787–1797; Y. Yang, F. Ding, J. Wu, X. Chen, J. Liu and X. Gu, *7th Asian-Pacific Conference on Medical and Biological Engineering IFMBE Proceedings*, 2008, pp. 4–8.
10 R. Langer and J. P. Vacanti, *Science*, 1993, **260**, 920–926.
11 P. C. Francel, K. S. Smith, F. A. Stevens, S. C. Kim, J. Gossett, C. Gossett, M. E. Davis, M. Lenaerts and P. Tompkins, *J. Neurosurg.*, 2003, **99**, 549–554; N. Weber, Y. S. Lee, S. Shanmugasundaram, M. Jaffe and T. L. Arinzeh, *Acta Biomater.*, 2010, **6**, 3550–3556; C. C. Gertz, M. K. Leach, L. K. Birrell, D. C. Martin, E. L. Feldman and J. M. Corey, *Dev. Neurobiol.*, 2010, **70**, 589–603; M. K. Horne, D. R. Nisbet, J. S. Forsythe and C. L. Parish, *Stem Cells Dev.*, 2010, **19**, 843–852.
12 S. Y. Chew, R. Mi, A. Hoke and K. W. Leong, *Biomaterials*, 2008, **29**, 653–661; H. S. Koh, T. Yong, C. K. Chan and S. Ramakrishna, *Biomaterials*, 2008, **29**, 3574–3582; L. Ghasemi-Mobarakeh, M. P. Prabhakaran, M. Morshed, M. H. Nasr-Esfahani and S. Ramakrishna, *Biomaterials*, 2008, **29**, 4532–4539; W. Li, Y. Guo, H. Wang, D. Shi, C. Liang, Z. Ye, F. Qing and J. Gong, *J. Mater. Sci.: Mater. Med.*, 2007, **19**, 847–854.
13 L. T. Lim, R. Auras and M. Rubino, *Prog. Polym. Sci.*, 2008, **33**, 820–852; S. S. Prakash, L. F. Francis and L. E. Scriven, *J. Membr. Sci.*, 2008, **313**, 135–157; T. van den Boomgaard, T. A. King, T. F. Tadros, H. Tang and B. Vincent, *J. Colloid Interface Sci.*, 1978, **66**, 68–76; S. Megelski, J. S. Stephens, D. B. Chase and J. F. Rabolt, *Macromolecules*, 2002, **35**, 8456–8466.
14 D. R. Salem, in *Nanofibre and Nanotechnology in Textiles*, ed. P. Brown and K. Stevens, Woodhead Publishing Ltd., Cambridge, UK, 2007.
15 M. Naraghi, S. N. Arshad and I. Chasiotis, *Polymer*, 2011, **52**, 1612–1618.
16 M. V. Kakade, S. Givens, K. Gardner, K. H. Lee, D. B. Chase and J. F. Rabolt, *J. Am. Chem. Soc.*, 2007, **129**, 2777–2782; T. Kongkhlang, K. Tashiro, M. Kotaki and S. Chirachanchai, *J. Am. Chem. Soc.*, 2008, **130**, 15460–15466.
17 T. Kondo and C. Sawatari, *Polymer*, 1996, **37**, 393–399; C. Y. Liang and R. H. Marchessault, *J. Polym. Sci.*, 1959, **39**, 269–278; L. M. Ilharco and R. Brito De Barros, *Langmuir*, 2000, **16**, 9331–9337; J. W. Park, T. Tanaka, Y. Doi and T. Iwata, *Macromol. Biosci.*, 2005, **5**, 840–852; L. M. Ilharco, A. R. Garcia, J. Lopes Da Silva and L. F. Vieira Ferreira, *Langmuir*, 1997, **13**, 4126–4132.